Astrometric Microlensing
Supervised Learning Project

Aravind Bharathi
Department of Physics
190260009

Supervisor: Professor Vikram Rentala

October 2021

Abstract

If dark matter is made up of primordial black holes (PBHs) then these black holes should be scattered all over the galaxy. As stars pass behind these PBHs, their light would get bent around the PBH due to an effect known as gravitational lensing. Modern space telescopes can detect tiny glitches in the apparent trajectories of these stars due to this lensing effect. The goal of this project is to explore the sensitivity of these space telescopes to different masses of PBHs with an emphasis on observations in the gamma radiation spectrum.

Contents

1 Introduction

Microlensing is an astronomical phenomenon due to the gravitational lensing effect. They have typically been used to detect objects that range from the mass of a planet ($\sim 10^{-6} M_\odot$) to the mass of a star ($\sim 10 M_\odot$)[1], regardless of the light they emit. Typically, only bright objects that emit much light (stars) or large objects that block background light (clouds of gas and dust) can be detected. These masses make up only a minor portion of the mass of a galaxy. Microlensing allows the study of objects that emit little or no light.

When a distant source of light gets sufficiently aligned with a massive compact foreground object, the bending of light due to its gravitational field, as discussed by Einstein in 1915, leads to two undistorted images. Microlensing deals with the case when these two images are unresolved, resulting only in an observable increase in flux or luminosity. The time-scale of the transient brightening depends on the mass of the foreground object as well as on the relative proper motion between the background 'source' and the foreground 'lens' object.

Typically, the source object in a microlensing system is dramatically brighter than the lens object, hence, contributions from the lens, known as the blending effect, are neglected. Microlensing therefore allows one to study massive objects no matter how faint. It is thus an ideal technique to study the galactic population of such faint or dark objects as brown dwarfs, planets, neutron stars, black holes and massive compact halo objects (MACHOs).

This report encapsulates the work done towards reproducing the results of a published article [3] that incorporates a novel technique known as the "lensing parallax" to model microlensing observations involving more sensitive measurements specifically for lower, previously unconstrained, lens mass ranges.

2 Overview on Gravitational Lensing

Newtonian mechanics predicts the deflection of light, however, the predicted value is only half of that predicted by General Relativity. Although Einstein's Field Equations can be used to calculate the exact null geodesics for light after modelling the spacetime metric around the lens, in lensing systems which involve very large distances, the lensing effect itself can be limited to a small region of spacetime around the lensing object and modelled using the central force problem.

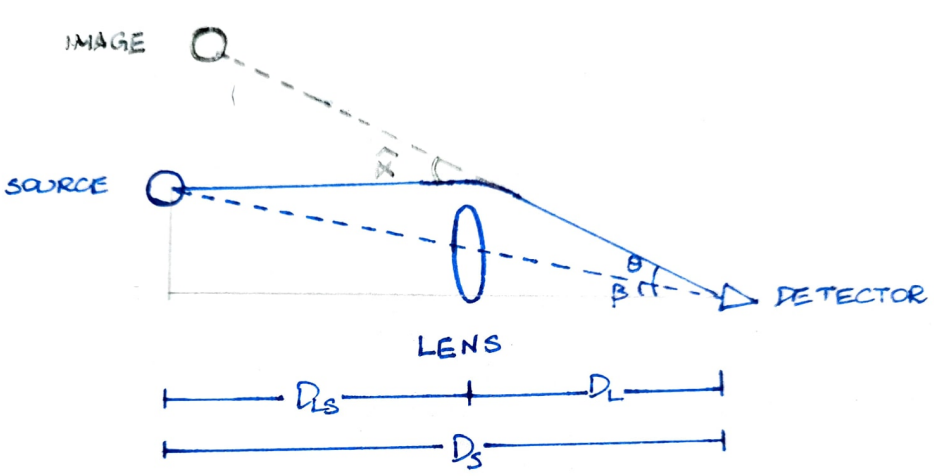

Figure 1: Deflection Angle

The deflection is thus the integral over the the 'pull' of the gravitational potential perpendicular to the light path $\vec{\nabla}\phi$ that points away from the lens.

$$\hat{\vec{\alpha}} = -\int_{\lambda_A}^{\lambda_B} \ddot{\vec{x}}\, d\lambda = \frac{2}{c^2}\int_{\lambda_A}^{\lambda_B} \vec{\nabla}_\perp \phi\, d\lambda \tag{1}$$

where x is the geodesic path of light parametrised by λ with end points A at the source and B at the observer, such that $x \equiv x(\lambda)$, $\phi = -GM_{lens}/r^2$ is the gravitational potential with r the displacement between the path and position of the lensing object.

If the mass of the lens is sufficiently small such that $\phi/c^2 \ll 1$, then $\hat{\vec{\alpha}}$ is also very small. Using methods from classical scattering theory, the integral can be approximated as,

$$\hat{\vec{\alpha}}(b) = \frac{4GM}{c^2}\frac{1}{b} \tag{2}$$

where b is the distance of closest approach, also known as the impact parameter[1].

Further sections are developed under the aforementioned approximations, henceforth, the gravitational lensing effect is described using a simple geometric ray tracing models.

2.1 Lens Equation

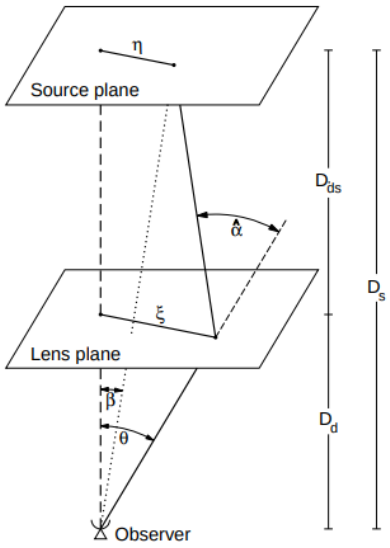

Figure 2: A Typical Gravitational Lensing System. *Reproduced from [2]*

Here, the source and lens planes are planes perpendicular to the optical axis of the detector containing the source and lens (approximated to a point) respectively, η and ξ are the positions of the source and lens relative to the source and lens planes respectively, D_L is the distance of the lens plane from the detector, D_S is the distance of the source plane from the detector and D_{LS} is the distance between the lens and source planes, β is the angular position of the source, θ is the apparent angular position of the source (i.e., the angular position of the image of the source) and $\hat{\alpha}$ is the deflection angle.

If the shape of the universe is globally flat, then $D_{LS} = D_S - D_L$. Further if the angles are small, then $\vec{\eta} \approx D_S\vec{\beta}$ and $\vec{b} \equiv \vec{\xi} \approx D_L\vec{\theta}$. It trivially follows that

$$\hat{\vec{\alpha}}D_{LS} = \vec{\theta}D_S - \vec{\beta}D_S \tag{3}$$

This is known as the lens equation. Using the geodesic equation 2, $\hat{\vec{\alpha}}$ can be written as

$$|\hat{\vec{\alpha}}| = -\frac{4GM}{c^2}\frac{1}{D_L\theta} \tag{4}$$

The lens objects under investigation here are predominantly compact objects and these are usually well approximated by an axially symmetric, point mass. For such objects, a characteristic scale called the Einstein angle θ_E can be described as follows

$$\theta_E = \sqrt{\frac{4GM}{c^2}\frac{1}{D}} \tag{5}$$

where the effective lensing distance D is defined as $D = D_L D_S/D_{LS}$. This allows the lens equation to be rewritten in a dimensionless (scalar) form by introducing parameters $\vec{x} = \vec{\theta}/\theta_E$, $\vec{u} = \vec{\beta}/\theta_E$

$$\Rightarrow u = x - \frac{1}{x} \tag{6}$$

[1]Note that this deflection angle exceeds the calculation from Newtonian gravity by a factor of two

with the roots at

$$x_{\pm} = \frac{1}{2}(u \pm \sqrt{u^2+4}) \Leftrightarrow \theta_{\pm} = \frac{1}{2}(\beta \pm \sqrt{\beta^2 + 4\theta_E^2}) \tag{7}$$

The magnification μ of an image is defined as the determinant of the inverse of the Jacobian matrix (defined by $\mathbf{J} = \partial\vec{u}/\partial\vec{x}$). This gives the following result

$$\mu_{\pm} = \left| \frac{1}{2} \pm \frac{(u^2+2)}{2u\sqrt{u^2+4}} \right| \tag{8}$$

Finally, the observed magnification for unresolved images is

$$A = \mu_+ + \mu_- + \sqrt{\mu_+\mu_-} \cos \frac{2\pi \Delta x_{path}}{\lambda} \tag{9}$$

where the last term comes from the wave nature of light, Δx_{path} being the difference in path travelled by the light rays of the two images and λ being the wavelength of electromagnetic radiation. Since, these astrophysical phenomena take place over large distances, $\lambda \ll \Delta x_{path}$, the time-averaged, observed magnification at the detector is simply

$$A = \mu_+ + \mu_- = \frac{(u^2+2)}{u\sqrt{u^2+4}} \tag{10}$$

For an unlensed flux F from the source, F' denotes the luminosity of the lensed observation. As the two images are unresolved in microlensing observations, the flux detected during a lensing event is

$$F' = AF \tag{11}$$

3 Lensing Parallax

Lensing parallax is a subset of microlensing observations which relies on simultaneous observations from spatially separated detectors, while doing away with the need for temporal data from transients (that take in the order of weeks). Here, one quantifies the differences in observations from the two detectors, to derive meaningful information from the data.

The goal of the paper under consideration [3] is to derive further constraints on the possible mass ranges of primordial black holes (PBHs) as a candidate to explain dark matter, and focuses on the range between $10^{-16} \lesssim M/M_{\odot} \lesssim 10^{-11}$. Previous studies [1, 4]($10^{-7} \leq M/M_{\odot} \leq 10^{1}$) and [5] ($10^{-11} \leq M/M_{\odot} \leq 10^{-6}$) have already narrowed down the possible windows for PBHs using observed radiation in the visible spectrum. On the other hand, the "GRB Lensing Parallax" paper uses high-energy electromagnetic radiation in the form of gamma-ray bursts (GRB) from very distant sources, and models objects distributed between the observer at Earth and these GRB progenitors as possible gravitational lenses. However, as these bursts only last from ten milliseconds to several hours, they cannot be detected using traditional microlensing methods. Instead, the paper employs the Lensing Parallax method to draw constraints on the possible nature and PBH composition of the lens.

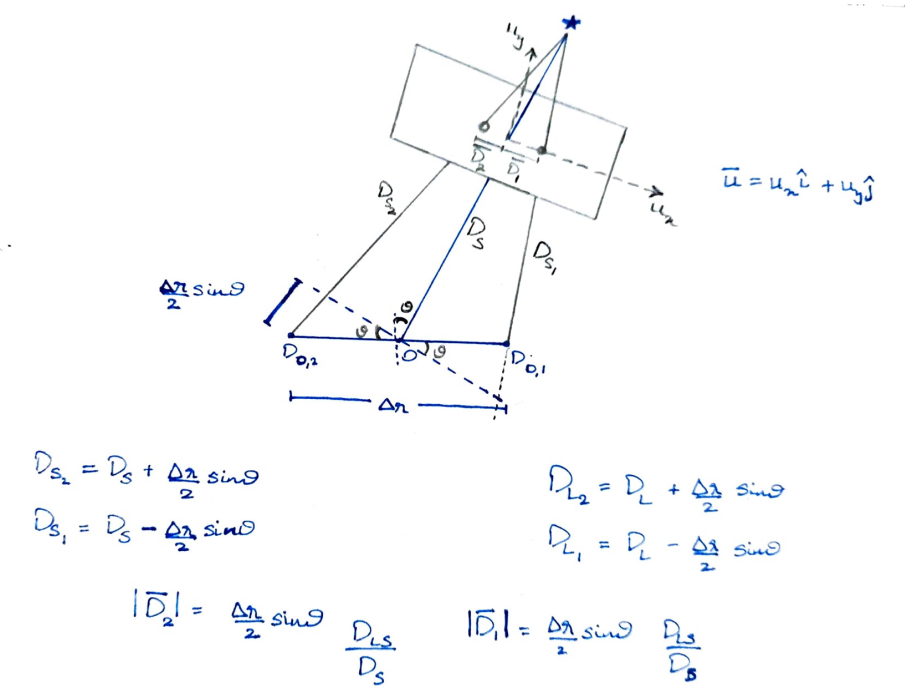

Figure 3: Typical Lensing Parallax System

The observed magnifications at detectors 1 and 2 are taken to be A_1 and A_2 respectively. A parameter *Obs* is defined as the observable in these Lensing Parallax events

$$Obs = \frac{|A_1 - A_2|}{\left(\frac{A_1+A_2}{2}\right)} \tag{12}$$

3.1 Necessary Conditions

To employ lensing parallax, the following conditions need to be met:

1. The detector separation Δr should be larger than the Einstein radius $r_E = D_L\theta_E$ of the lens

$$\Delta r \gtrsim r_E \Leftrightarrow \left(\frac{M}{10^{-7}M_\odot}\right) \lesssim \left(\frac{\Delta r}{AU}\right)^2 \left(\frac{D}{Gpc}\right)^{-1} \tag{13}$$

   The Einstein radius is a characteristic length scale in gravitational lensing events: From equation 7, it can be seen that one image lies slightly within θ_E and the other image lies slightly outside θ_E. This implies that over a distance of $\sim 2r_E$ (or $2\theta_E$), the observed magnification changes significantly. Therefore, detectors separated by distances greater than this characteristic length can simultaneously observe the two different 'periods' of the transient in a traditional microlensing event (i.e, peaked magnification and non-peaked magnification).

2. The changes in observed magnification needs to be detectable by the sensor and this follows from the radiometric resolution[2] of a sensor. Effectively, the observable *Obs* must be more different than the resolution

$$Obs \gtrsim \epsilon$$

   A finite apparent source angular size $\theta_S \approx r_S/D_S$ (where r_S is the physical transverse emission radius) is taken into account, instead of the previous point-like source approximation (the lens is still approximated as a point). This leads to a more involved calculation for magnification as shown in [6]: A parameter δ is defined as $\delta = \theta_S/\theta_E$ which characterises the relative size of the source with respect to the Einstein angle. δ needs to

[2]Radiometric resolution refers to the number of discrete levels of flux that can be detected by a sensor. For example, a 10 bit sensor can output values from 0 to 1023 depending on the flux-output calibration of the sensor

be small to induce sizable lensing effects, as otherwise, only a small part of the source will be magnified. The key magnification results from [6] are

$$A(u,\delta) \approx \begin{cases} A_{in}(u,\delta) & \text{for } u < \delta \\ A_{out}(u,\delta) & \text{for } u > \delta \end{cases} \tag{14}$$

where

$$A_{in}(u,\delta) = \sqrt{1+\frac{4}{\delta^2}} - \frac{8}{\delta^3(\delta^2+4)^{1.5}}\frac{u^2}{2} - \frac{144(\delta^4+2\delta^2+2)}{\delta^5(\delta^2+4)^{3.5}}\frac{u^4}{24}$$

$$A_{out}(u,\delta) = \frac{2+u^2}{u\sqrt{u^2+4}} + \frac{8(u^2+1)}{u^3(u^2+4)^{2.5}}\frac{\delta^2}{2} + \frac{48(3u^6+6u^4+14u^2+12)}{u^5(u^2+4)^{4.5}}\frac{\delta^4}{24}$$

[3] states that A_{in} and A_{out} respectively overestimates and underestimates the actual magnification value at $y \approx \delta$. Hence, for $0.9\delta < u < 1.1\delta$, the two endpoints are linearly interpolated such that

$$A = A_{out}(1.1\delta,\delta)\frac{(u-0.9\delta)}{0.2\delta} + A_{in}(0.9\delta,\delta)\frac{(1.1\delta-u)}{0.2\delta}$$

As described above, considering large δ does not induce sizable lensing effects, in the limit $\delta \gtrsim 1$, the following constraint is drawn

$$\left(\frac{M}{10^{-12}M_\odot}\right) \gtrsim \epsilon \left(\frac{r_S}{r_\odot}\right)^2 \left(\frac{D}{Gpc}\right)^{-1} \tag{15}$$

At the limit $\delta \to 0$, the magnification expression for the point source approximation, as shown in equation 10, is recovered.

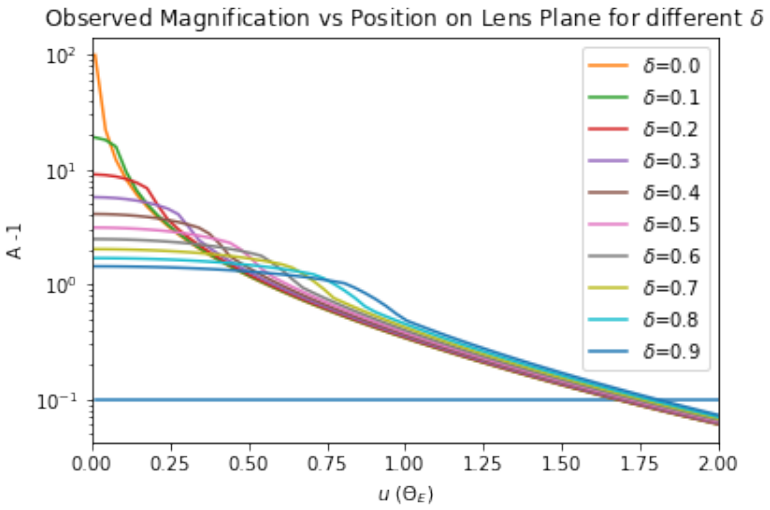

Figure 4: Magnification values $(A-1)$ depicted for different values of δ. Note that $\delta = 0$ represents the point source approximation and the blue line represents a weaker, necessary condition on A_i $i = 1, 2$ 4.4. The latter therefore sets a threshold on u beyond which no changes can be detected by a sensor with $\epsilon = 0.1$

3. Finally, the probe wavelength λ must be shorter than the Schwarzschild radius of a PBH lens, otherwise, the wave cannot see the lens → geometrical optics approximation is valid for

$$\lambda \ll \frac{2GM}{c^2}(1+z_L) \tag{16}$$

The paper translates the much less than symbol as at least one order in magnitude (as an ad hoc for numerical calculations), while the lens redshift factor describes the wavelength of light as it was passing by the lens (at a time in the past, since the wavelength observed at the detector has been further cosmologically redshifted due to the expansion of space)

Based on these conditions, gamma radiation with energy $50keV$ to $5MeV$ can be used to derive constraints on PBH masses between $10^{-16} \lesssim M/M_{\odot} \lesssim 10^{-11}$.

4 Deriving Bounds on PBH Composition in DM

4.1 Distance Measures

The paper cites GRBOX[3] for the distribution of GRB progenitors by the amount of their redshift. The comoving distance to these sources D_S can then be obtained through the FLRW metric

$$D_S = \int_0^z \frac{c\, dz}{H(z)} \tag{17}$$

where

$$H(z) = H_0 \sqrt{\Omega_{Matter}(1+z)^3 + \Omega_{Radiation}(1+z)^4 + \Omega_{\Lambda}}$$

and H_0 is the cosmological constant

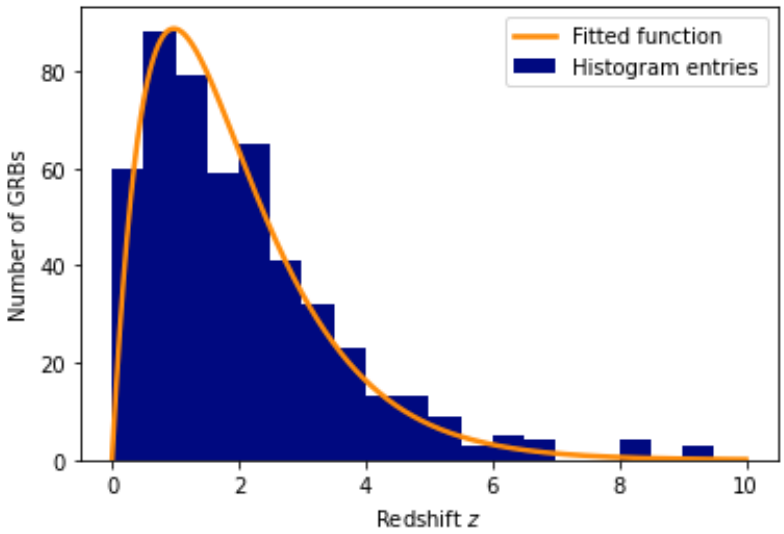

Figure 5: Distribution of Redshift vs # GRB

[3]GRBOX: Gamma-Ray Burst Online Index, https://sites.astro.caltech.edu/grbox/grbox.php

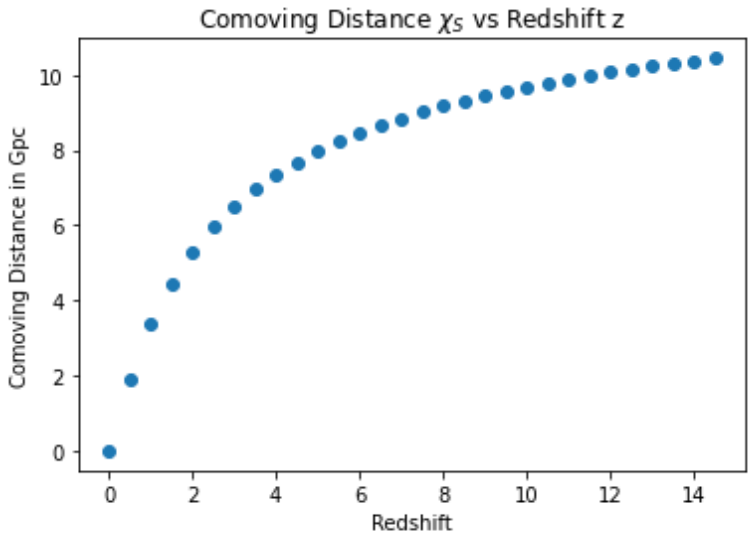

Figure 6: Redshift vs Comoving Distance

4.2 Source Size Measures

The paper once again cites GRBOX for the distribution of the number of GRB progenitors by source size

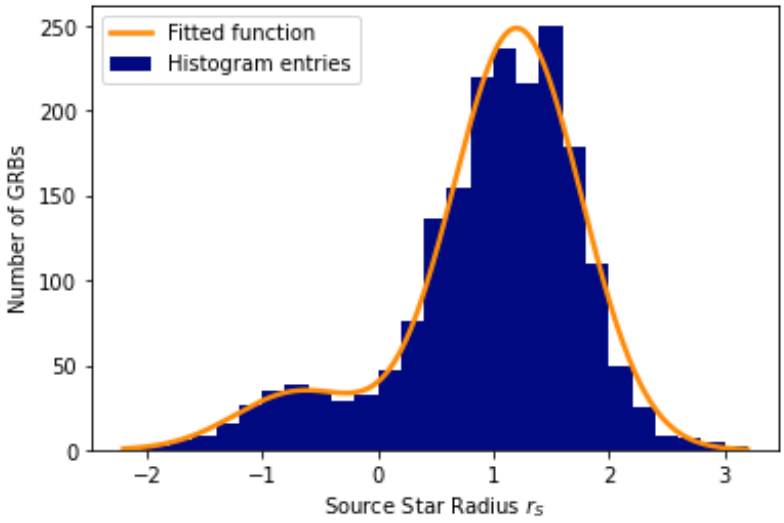

Figure 7: Distribution of source radius vs # GRB

4.3 Point Source vs Finite Source Size Effect

The difference between the observed magnifications using the point source approximation versus taking the finite source radius r_S into account results in the following plots. The other parameter values are $\epsilon = 0.1, r_S = 0.1 r_\odot$

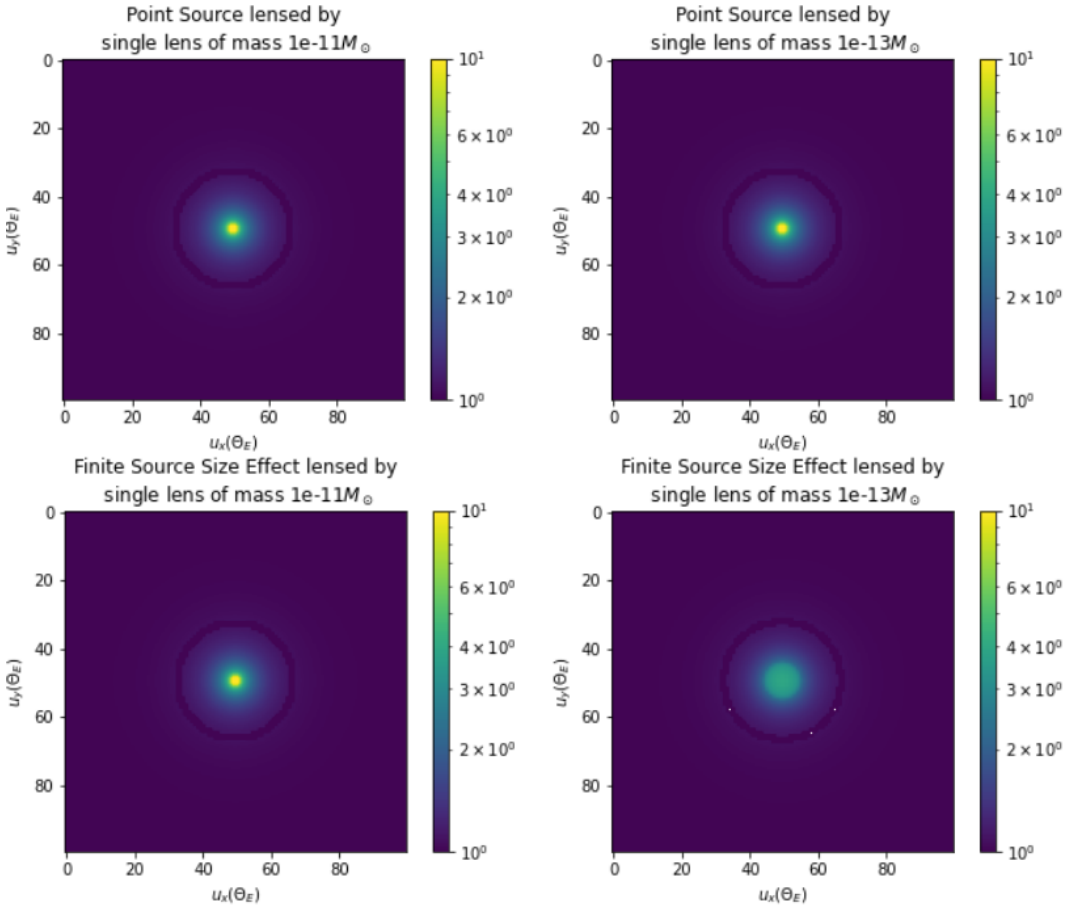

Figure 8: Point Source vs Finite Source Size Effect

The faint circle represents the contour of detectable regions of the observed magnifications based on criteria 4.4

4.4 Cross Section Area of Lenses

The field of view of each detector is broken down into a grid of $n \times n$ discrete cells. Cells which satisfy the condition in equation 2 will be considered as bright cells. A weaker relation to equation 2 can be stated as

$$A_1 \vee A_2 > 1 + \epsilon$$

which can be used to quickly discard cells that will not satisfy the condition in equation 2. Eventually, the cross section area σ occupied by the bright cells represent the region of detectable lensing events. The number of cells was taken to be $80 \times 80 = 6400$ in [3]. Nevertheless, increasing n increases the resolution of these discrete cells and are expected to give more refined results.

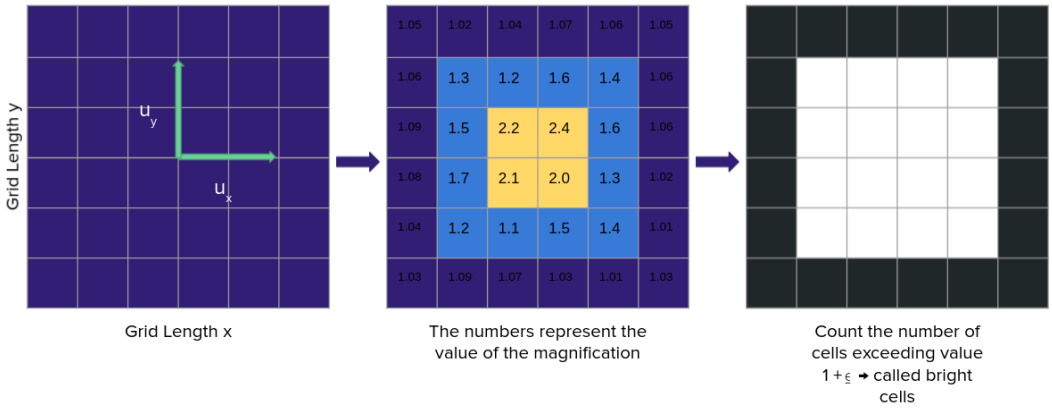

Figure 9: Cross Section Area as observed within the Field of View of a single detector

The observable *Obs* measured using magnifications from both the detectors can be used to find the cross section area occupied by bright cells

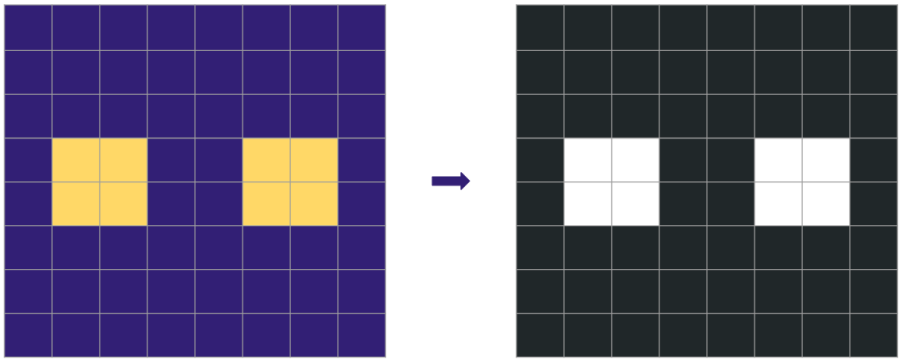

Figure 10: Cross Section Area as measured within the Field of View of two detectors

4.4.1 Simulated Results

The current setup can be used to simulate the cross section by varying multiple parameters:

1. ϵ
2. Size of the GRB progenitor
3. Mass of the lens
4. Separation of the detectors
5. Distance to the source
6. Distance to the lens
7. Number of discrete cells in the cross section grid
8. Side length of the grid
9. Tilt of the orbit with respect to source (Not modelled in [3]. Refer 5)

The side length of the grid (currently specified in units of θ_E) and the number of cells in the grid are used to determine the width of each cell. Intermediate values *tmp_x* and *tmp_y* (corresponding to u_x and u_y in figure 9), representing the distance of a cell from the centre of the grid, are calculated by first recentering the origin of the

cross section from the top left cell (which follows from typical array indexing) to the centre of the grid and then scaling the length by the cell width.

$$tmp\_x = ((i - n/2) + 0.5) \times \text{cell width} \quad tmp\_y = ((j - n/2) + 0.5) \times \text{cell width} \tag{18}$$

where (i, j) is the array index of the cell under consideration. Next, the angular position of the source β as seen from the two detectors are calculated by the Pythagoras' theorem

$$\beta_1 = \sqrt{(tmp\_x - \frac{\Delta r}{2D})^2 + tmp\_y^2} \quad \beta_2 = \sqrt{(tmp\_x + \frac{\Delta r}{2D})^2 + tmp\_y^2} \tag{19}$$

where $\Delta r/D$ represents the effective projection of the detectors on the lens plane. Finally,

$$u_1 = \frac{\beta_1}{\theta_E} \quad u_2 = \frac{\beta_2}{\theta_E} \tag{20}$$

This, along with the source radius, permits the calculation of the observed magnification $A(u, \delta)$ as shown in equation 14. This process is performed at every cell from which the *Obs* is calculated using equation 12.

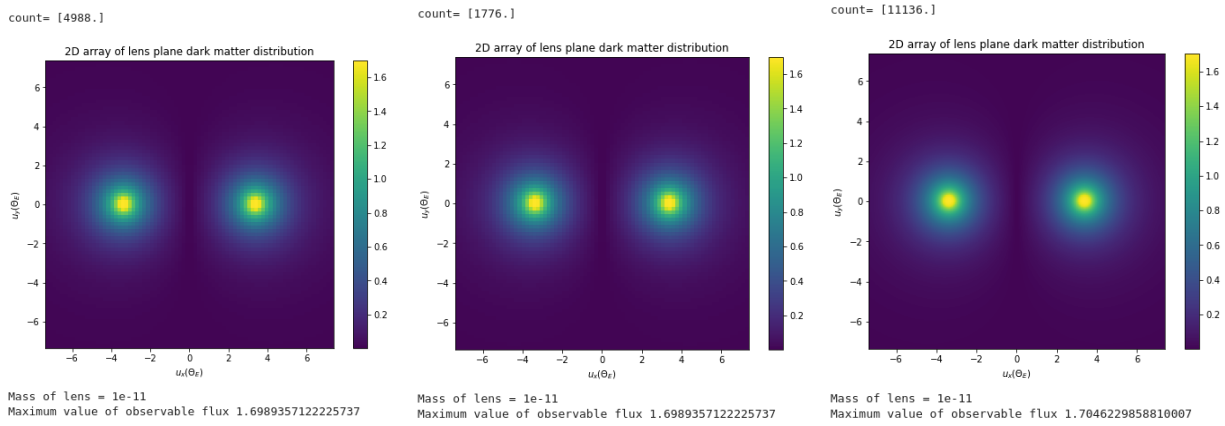

(a) Parameter values:
$\epsilon = 0.01$
Grid length = Δr/D + $4\theta_E$
Number of cells = 80x80 = 6400

(b) Parameter values:
$\epsilon = 0.1$
Grid length = Δr/D + $4\theta_E$
Number of cells = 80x80 = 6400

(c) Parameter values:
$\epsilon = 0.1$
Grid length = Δr/D + $4\theta_E$
Number of cells = 200x200 = 40000

Figure 11: The simulated distribution of observable values on the grid; count represents the number of bright cells detected in the grid

The cross section area is calculated by

$$\sigma = \#\text{bright cells} \times \text{area of one cell} \tag{21}$$

4.5 Volume Occupied by Lenses

Finally, the volume V_L occupied by these lenses can be calculated by integrating over the complete region between detector and source. A quantity $x_{lens} = D_L/D_S$ is usually defined to carry out the integration.

$$V_L(D_S; r_S, \epsilon) = \int_0^{D_S} \sigma(x_{lens}; r_S, \epsilon) dx_{lens} \tag{22}$$

As these integrations are carried out numerically, the quadrature formula is used by stacking multiple cross sections at different distance $0 \leq x_{lens} \leq 1$. This volume is also referred to as the comoving volume for lenses.

Implemented Procedure The code utilises the *Obs* obtained from section 4.4 and counts the number of cells which are bright (i.e., satisfy equation 2). The area occupied by these bright cells $\sigma(x_{lens})$ is calculated by multiplying the number of bright cells by the area of each cell. Using the midpoint quadrature formula, V_L is calculated as follows

$$V_L = h(\frac{1}{2}\sigma(a) + \sigma(a + h) + \sigma(a + 2h) + \ldots \frac{1}{2}\sigma(b)) \tag{23}$$

where $h = (b-a)/(\#cross\ sections - 1)$ is the distance between two calculated cross sections; a and b are the start and end distances in these 'stacked' cross sections. Here, the number of intervals can be varied as per the need (the original paper uses 24 cross sections). This translates to $a = 0.04$ and $b = 0.96$.

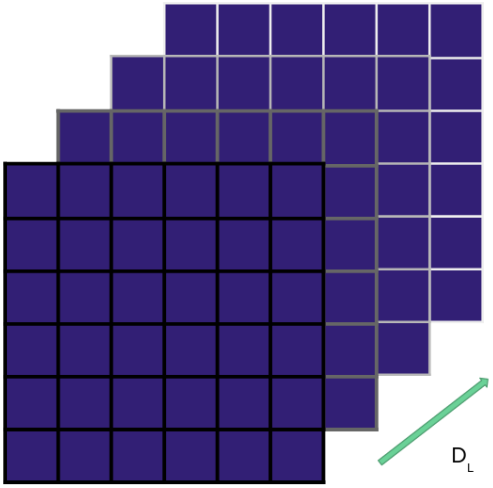

Figure 12: Volume Occupied by Lenses

The plot between the area occupied by bright cells in each cross section and the distance from the detector for a lens mass $10^{-11} M_{\odot}$ and $\epsilon = 0.1$ is shown below

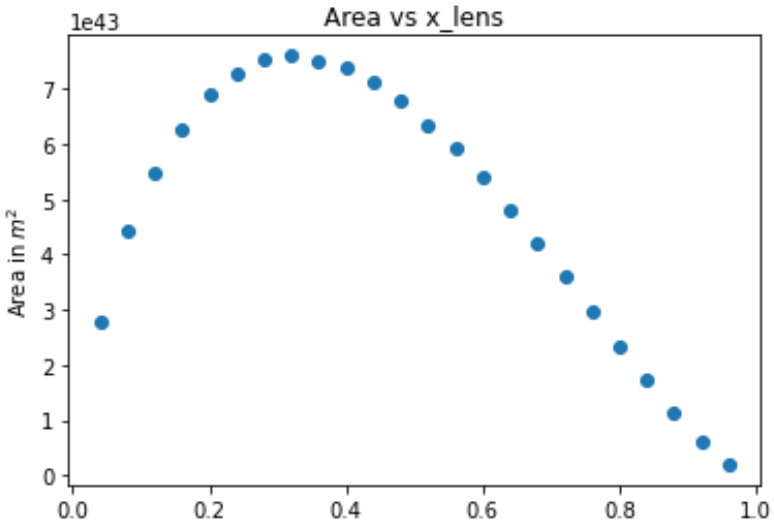

Figure 13: Area of Cross Section vs x_{lens}

4.6 Optical Depth

The optical depth is a measure of transparency of the medium. It is calculated by

$$\tau(D_S; f; M; r_S, \epsilon) = \int n(f; M)\ dV_L(D_S; r_S, \epsilon) \tag{24}$$

where n is the comoving number density. There may be large local variations in n but globally it has been approximated to $n \approx \rho_{crit,0}\Omega_{DM} f/M$ with $\rho_{crit,0} = 3H_0^2/8\pi G$ and $f = \Omega_{PBH}/\Omega_{DM}$.

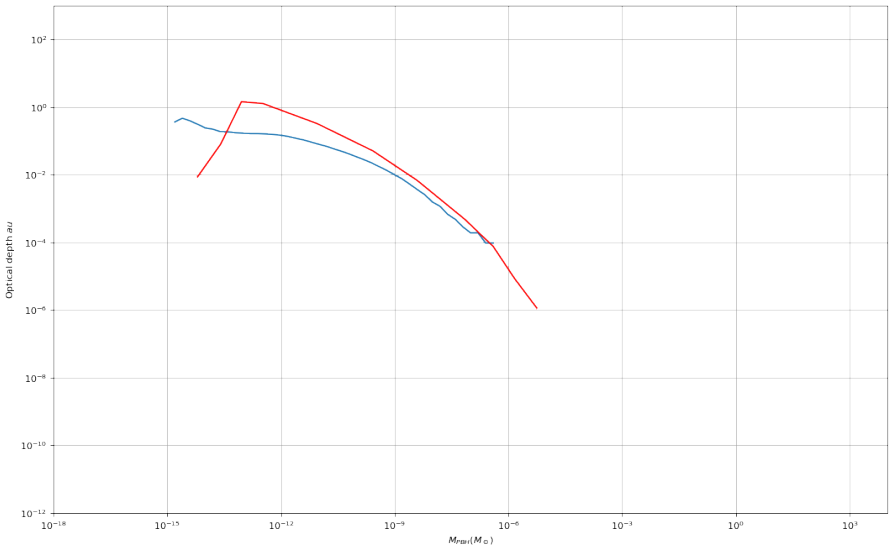

Figure 14: Simulated optical depth (blue) overlayed on the plot reproduced from [3] (red)
Parameter values: $z_S = 2$, $\Delta r = L_2$, $\epsilon = 0.1$, $r_S = r_\odot$
The code can be found at https://github.com/aravindbharathi/Astrometric-Microlensing. The discrepancy is speculated to have arisen due to some bugs in the code. Refer 4.8

4.7 Deriving Exclusion Graphs

4.7.1 Probability of Lensing

The probability of lensing follows a Poisson distribution over the optical depth

$$\mathcal{P}(\alpha) = \frac{\tau^\alpha e^{-\tau}}{\alpha!} \tag{25}$$

where α is the number of lensing events per detection. To maximise the the probability of single lensing event, i.e., $\alpha = 1$, τ needs to be 1.

4.7.2 Probability of Null Detection

The probability of more than 2 lensing events is expected to be negligibly small. From figure 14, the optical depth can be seen to be lower than 10. The probability depends on the optical depth, thereby implicitly dependent on the comoving volume and PBH abundance (f) $\Rightarrow \mathcal{P} \equiv \mathcal{P}(\alpha, f)$. Say $\tau = 10^{-2}$, then $\mathcal{P}(0,1) = 0.99$, $\mathcal{P}(1,1) = 0.0099$, $\mathcal{P}(2,1) = 4.95 \times 10^{-5}$. Hence, $\mathcal{P}(0,f)$ can be well approximated by

$$\mathcal{P}(0,f) \cong (1 - \mathcal{P}(1,f)) \tag{26}$$

Let $P_{Null}(f)$ represent the probability of lensing event for multiple sources sampled from the aforementioned GRB distributions then it represents the following

$$P_{Null}(f) = \Pi_i \mathcal{P}_i(0,f) \tag{27}$$

where the product is over the sampled GRBs. Statistically, if $P_{Null} < 0.05$, no detections are reported.

Hence, f is bounded by finding $P_{Null} \geq 0.05$ and this is termed the "criteria for exclusion"

4.7.3 Exclusion Curves

The modelling of these exclusion curves incorporates various distributions of GRBs as mentioned before - although, they are not limited to the source star's radius 4.2 and distance from observer 4.1. Other distributions such as the tilt of the plane of the orbit can be included, refer section 5.

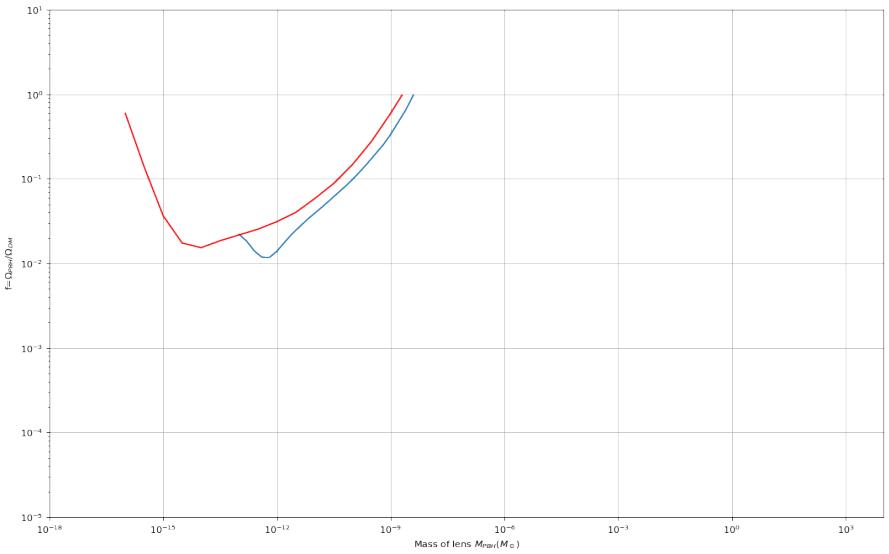

Figure 15: Simulated exclusion curve (blue) overlayed on the plot reproduced from [3] (red)
Parameter values: $\Delta r = L_2$, $\epsilon = 0.1$
The code can be found at https://github.com/aravindbharathi/Astrometric-Microlensing. The discrepancy propagates from the possible bug in the optical depth implementation 4.6. This needs to be investigated further

4.8 Future Work

1. Fix a bug in the projection of detectors onto lens plane (overall results may scale up or down by less than an order of magnitude)
2. Fix a bug in volume calculation (there is some mismatch in variable assignment; overall results may change by more than an order of magnitude)
3. Optimise the implemented code
4. Obtain similar plots for other detector separations ($\Delta r = r_\oplus, AU$)
5. Investigate and address research gaps 5
6. From previous discussions:
    - Calculate the observed time delay between twin satellites at low earth orbit (to model Daksha)
    - Study femtolensing and its effects

5 Research Gaps

1. Incorporate the distribution of tilt orbit vs GRB progenitors 4.7.3
2. Wave optic effects could be accounted for at lower lens masses
3. Investigate the effect of polarisation of light
4. Observation of parallax in binary stars where the source has detectable motion
5. From previous discussions:
    - Investigate the effects of $\rho_{crit} \gg \rho_{crit,0}$ inside the Milky Way galaxy on the calculation of co-moving number density and subsequent calculations of optical depth and exclusion curves

References

[1] C. Alcock, R. A. Allsman, D. R. Alves, T. S. Axelrod, A. C. Becker, D. P. Bennett, K. H. Cook, N. Dalal, A. J. Drake, K. C. Freeman, and et al. The macho project: Microlensing results from 5.7 years of large magellanic cloud observations. *The Astrophysical Journal*, 542(1):281–307, Oct 2000.

[2] Matthias Bartelmann and Peter Schneider. Weak gravitational lensing. *Physics Reports*, 340(4-5):291–472, Jan 2001.

[3] Sunghoon Jung and TaeHun Kim. Gamma-ray burst lensing parallax: Closing the primordial black hole dark matter mass window. *Physical Review Research*, 2(1), Feb 2020.

[4] M. Moniez. Review of results from eros microlensing search for massive compact objects, 2009.

[5] Hiroko Niikura, Masahiro Takada, Naoki Yasuda, Robert H. Lupton, Takahiro Sumi, Surhud More, Toshiki Kurita, Sunao Sugiyama, Anupreeta More, Masamune Oguri, and et al. Microlensing constraints on primordial black holes with subaru/hsc andromeda observations. *Nature Astronomy*, 3(6):524–534, Apr 2019.

[6] Hans J Witt and Shude Mao. Can lensed stars be regarded as pointlike for microlensing by machos? *The Astrophysical Journal*, 430:505–510, 1994.

Appendix

Packages Used

1. `numpy`
2. `matplotlib: pyplot`
3. `scipy: optimize.curve_fit, optimize.newton, integrate.quad`
4. `PIL`
5. `astropy: cosmology.WMAP9`

Constants Used

- Speed of light: $c = 3 \cdot 10^8 \frac{m}{s}$
- Astronomical unit: $AU = 1.5 \cdot 10^{11} m$
- Gravitational constant: $G = 6.67 \cdot 10^{-11} \frac{m^3}{kg\ s}$
- Parsec: $pc = 3 \cdot 10^{16} m$
- Giga parsec: $Gpc = 3 \cdot 10^{25} m$
- Hubble's constant: $H_0 = 70 \cdot 10^3 \frac{m}{s\ Mpc}$
- Mass of sun: $M_\odot = M\_sun = 2 \cdot 10^{30} kg$
- Radius of sun: $r_\odot = r\_sun = 7 \cdot 10^8 m$
- Critical density of the Universe: $\rho_{crit,0} = 3H_0^2/8\pi G = 9.21 \cdot 10^{-27} kgm^{-3}$
- Energy density of Dark Energy: $\Omega_\Lambda = 0.7$
- Energy density of Matter: $\Omega_\Lambda = 0.03$
- Energy density of Dark Matter: $\Omega_\Lambda = 0.26$

Code Repository The code developed to run the simulations and reproduce calculations may be found here: https://github.com/aravindbharathi/Astrometric-Microlensing/